Swimming modes & interactions of anisotropic active colloids

Riedel, S.M.I.

Chapter 3

Shape-dependent direction reversal in anisotropic catalytic microswimmers

3.

The propulsion direction of active particles is a key feature in self-propelled systems and has been shown to depend on the propulsion mechanism and environmental conditions. Here, using 3D micro-printed catalytically active particles, we experimentally demonstrate that the propulsion direction can change with increasing fuel concentration when the active particle possesses an anisotropic shape.

We find that discs, tori, and bent rods reverse their direction of motion with increasing hydrogen peroxide concentration — moving with their inert side forward at low concentrations and with their catalytic side forward at high concentrations. In contrast, spheres and side-propelling straight rods do not exhibit this reversal. We observe that the direction reversal occurs for different material compositions and sizes of anisotropic swimmers, only changing the hydrogen peroxide concentration at which reversal appears. We find that the propulsion direction is influenced by the interplay of pH-dependent surface zeta potential, particle geometry, and substrate-induced solute confinement.

This chapter is based on the following article:

Shape-dependent direction reversal in anisotropic catalytic microswimmers.
S. Riedel, M. Wei and D. J. Kraft
in review (2025)

3.1 Introduction

Catalytic active colloids are out-of-equilibrium synthetic systems that self-propel as a result of asymmetric solute gradients generated on the swimmer's surface[1–5]. Such chemically driven microswimmers are typically Janus particles[6] consisting of an inert and a catalytic side which are obtained by half-coating the particle with a metal catalyst. When dispersed in a fuel solution, the local decomposition of the fuel on the catalytic side generates non-uniform chemical fields around the particle that drive the motion of the swimmer[3]. Speed[7], directionality[8–10], and swimming modes[11] are important features of this autonomous propulsion and the key to controlling these systems.

The direction of propulsion of these Janus spheres is set by the location of the symmetry breaking metal coating and is parallel to the symmetry broken axis. Depending on the material of the catalytic cap the spheres either propel towards or away from the catalytic metal coating: Janus-spheres half coated with a thin platinum (Pt) layer typically swim inert side forward[12,13], while Janus-spheres with a copper (Cu) coating swim catalytic side forward due to an inversion of the surface zetapotential of the metal hemisphere by the release of Cu^{2+} ions[14]. In both cases, the respective direction of motion is constant at all fuel concentrations.

Reversing the propulsion direction, especially of anisotropic swimmers, dramatically changes the particle-particle interactions and consequently the collective behavior of the active system[15]. Predicting and controlling the direction of motion is therefore crucial when designing self-propelling units. However, a change in the direction of motion typically requires a different makeup of the particle. In 3D printed microtori, for example, different directionalities of the particle velocities were achieved by changing the chemical composition of the catalytic cap[16]. Direction reversal can similarly be induced by changes in the experimental conditions and surrounding fluid. For example, adjustments in the local pH can influence the direction in which a swimmer propels either by altering the dominant reaction that occurs at the catalytic cap[17] or by reversing the surface zeta potential[18]. Likewise, changes in the illumination intensity can reverse the swimming direction of photocatalytic micromotors by a shift in propulsion mechanism from self-diffusiophoresis to self-thermophoresis[19]. The addition of a cationic surfactant has furthermore been shown to reverse the propulsion direction of Pt-Janus microspheres and pure Pt-based rotors, because it inverts the surface charge of the particle, thereby leading to a reversal of the ionic current,[4,20].

Surprisingly, in our previous work on shape-dependent clustering of active particles, we found that crescent-shaped Janus-colloids exhibited opposite propulsion directions at different fuel concentration[15]. At low fuel concentrations the particles moved with their inert cavity forward while at high fuel concentrations they moved with their metal-coated rounded side forward. The reversal in propulsion direction observed in crescent-shaped particles did not stem from a different make-up of the particles but occurred only upon a change in fuel concentration. Moreover, a change of the environmental condition alone cannot explain why crescent-shaped particles would reverse. The reason is that despite extensive experiments on Pt-half coated Janus spheres driven by a catalytic decomposition of H_2O_2, no reports exist of a similar direction reversal in spheres suggesting that shape must play a decisive part.

Indeed, the particle shape of catalytic swimmers has been theoretically predicted to allow tuning of the propulsion direction. For anisotropic particle geometries, shape-induced effects on the diffusion and confinement of solutes can influence the near-field concentration gradients around the particle, and thus the orientation of the propulsive phoretic forces generated by the active site[20,21]. However, for any given shape, changing the propulsion direction was predicted to necessitate altering of the relative electrophoretic mobilities or activities of the two halves of the particle. Since the electrophoretic mobilities are linked to the zetapotential of the two halves through Smoluchowskis equation, this directly implies a dependence on the chemical properties of the particle halves. For spheres, direction reversal requires an inversion of the relative mobilities or zetapotentials of polymer and catalytic side, while for oblate shapes even small changes around relative zetapotentials of 1 can induce a direction reversal.

We here experimentally investigate how the particle shape can influence the swimming direction by examining active spheres, discs, tori, bend rods (crescents), and straight rods at different fuel concentrations. While all particles swim with their inert side leading at low fuel concentrations, we report a reversal of the swimming direction when the fuel concentration is increased for discs, tori and crescents but not for spheres and straight rods. We show that this reversal depends on their anisotropic shape and occurs for both particles made from polymers or silica and coated with Pt/Pd or Pt. We find that the fuel concentration at which direction reversal for these shapes is observed coincides with a change in pH, which affects the relative surface zetapotentials of the two halves of the particle. For anisotropic shapes which are sensitive to small relative changes this leads to a direction reversal, whereas for spheres and rods this does not. Using COMSOL simulations, we show that for particles of different shapes, additional confinement of solutes by the

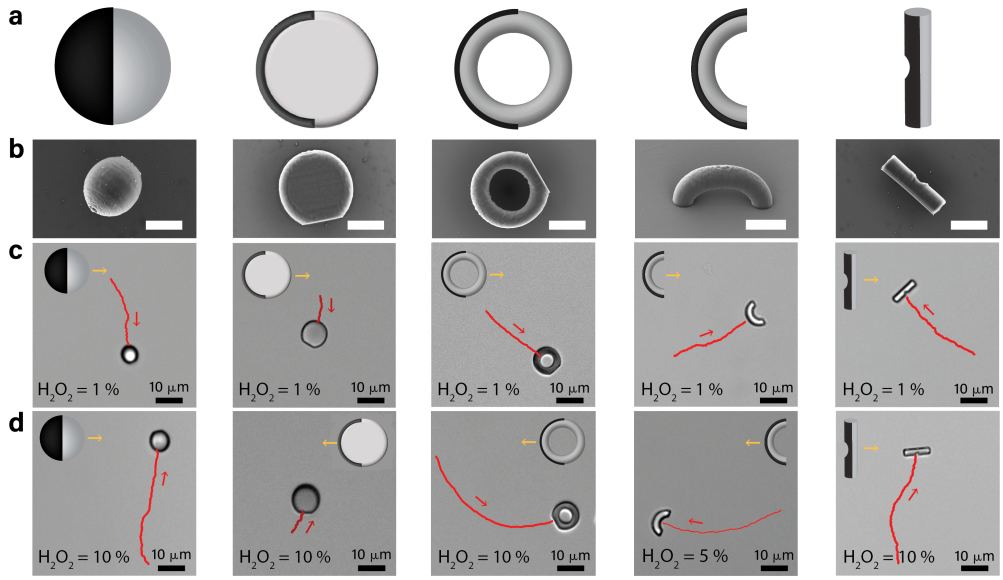

Figure 3.1: Shape- and fuel concentration dependent directionality of the propulsion direction. (a) Schematics, (b) scanning electron microscopy (SEM) images and (c-d) bright-field images with particle trajectory of 3D printed spheres, discs, tori, crescents and rods (left to right). The metal cap in the schematics is represented in black. The scale bar in the SEM images is 5 µm. A 30s trajectory traveled by the active particle is shown in red. At low fuel concentrations (1 wt% H_2O_2, c) all shapes swim inert-side forward. At higher fuel concentrations (10 wt% H_2O_2, d) a reversal of the swimming direction is observed for discs, tori and crescents but not for spheres and rods. Small shape defects stemming from cut-offs during printing or intentional introduction of a groove (rod-only) allow visual identification of the particle's inert side and thus its swimming direction.

substrate modifies the surrounding concentration field in a shape-dependent manner. Our insights provide the first methodological experimental study of a shape-dependent direction reversal stimulated by a change in fuel concentration.

3.2 Results and Discussion

Self-propelled 3D Microprinted Colloids. To understand the influence of the particle geometry on the swimming direction, we compare the individual particle behavior of microswimmers that differ only in their shape. We make use of an efficient and reproducible 3D microprinting technique based on two-photon polymerization to obtain monodisperse

anisotropic colloidal structures[15,22]. We print particles of five different shapes keeping their maximal extension constant at 10μm: spheres, discs, tori, crescents and rods (see Fig. 3.1 a and b, Appendix Fig. 3.8). This choice of shapes was made because they are linked through simple changes in their symmetry and topology while covering a wide range of basic shapes. These include the widely employed spheres, for which no direction reversal with changing H_2O_2 concentration has been reported thus far, and the crescents, for which we initially discovered the direction reversal. Spheres can be transformed into discs by reducing their z-dimension while tori are obtained from discs by introducing a cavity in the center of the structure. The torus structure is further halved to obtain a crescent (bend rod) and finally the crescent can be straightened into a rod, see the Materials and Methods section for more details on particle fabrication and particle dimensions, see Appendix for more details on the particle design.

We render all particles active by sputter coating them with a 5 nm thick Pt/Pd (80/20) layer (cf. schematic in Fig. 3.1 a and Appendix Fig. 3.9) and dispersing them in aqueous hydrogen peroxide (H_2O_2) solution. Self-propulsion in this system of synthetic catalytic microswimmers is driven by solute gradients generated through the catalytic decomposition of H_2O_2 at the Pt/Pd cap[1,3]. For spheres, discs, and tori the propulsion direction can be identified by localizing a shape defect that originates from the contact area that the particles had with the substrate during printing. For rods, the inert side is recognizable by a small groove on the top side of the particle which we added for this purpose during particle design.

Shape-dependent Swimming Direction and Direction Reversal. We start by testing which of these shapes, beside the crescents, show direction reversal and disperse our 3D printed particles in both low and high fuel concentrations. In 1 wt% H_2O_2 all particles move inert-side leading (Fig. 3.1 c). However, when increasing the fuel concentration to 10 wt% H_2O_2, we find that not only do crescents reverse their swimming direction, but also discs and tori now swim catalytic side forward, see Fig. 3.1 d and Supplementary Videos 1-10. The propulsion direction of the particles depends on the fuel concentration and is very stable; it is unaffected by later changes in fuel concentration suggesting a self-stabilizing effect such as is the case in a concentration gradient of fuel, see Appendix. As a control, we furthermore tested crescents that were sputter coated on their concave side. These particles also show both swimming directions depending on the fuel concentration, see Appendix Fig. 3.11. In line with literature, no direction reversal was observed for spheres and side-propelled rods when the fuel concentration was changed.

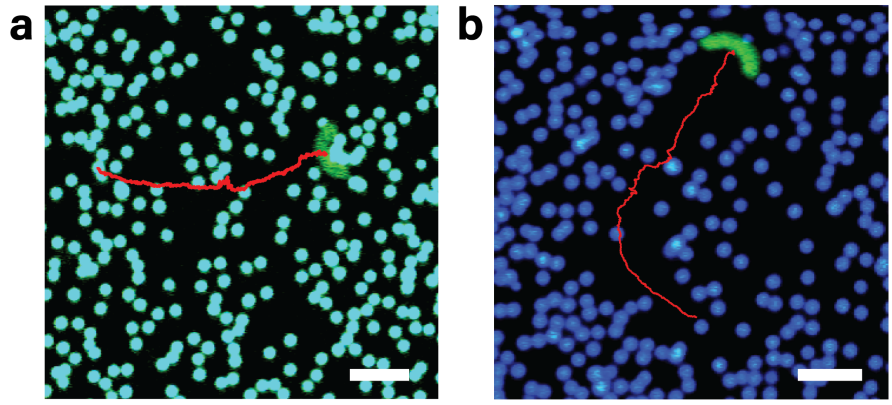

Figure 3.2: Interactions with tracer particles. 50 sec trajectory of crescent in a tracer particle bath. (a) Inert side leading crescent swimming at a velocity of 0.68 $\mu m/s$ in 1 wt% H_2O_2 and (b) metal-cap leading crescent swimming at a velocity of 1.07$\mu m/s$ in 10wt% H_2O_2. The tracer particles are TPM colloids with a diameter of 1.77 μm and the scale bar represents 10 μm respectively.

Unsurprisingly, the change in propulsion direction produces distinctly different flow profiles. To visualize these differences, we introduce 1.77-µm-diameter TPM tracer particles[23] and track their behavior near crescent particles moving polymer or metal side leading. The different interactions between the tracers and the swimmer in the two propulsion directions are clearly pronounced: cavity-forward moving crescents collect tracers in their cavity, yet do not leave a trail free of tracers due to the flow which sucks in tracers at their curved rear end, see Fig. 3.2 and the Supplementary Videos 11 and 12. In contrast, a curved-side forward moving crescent does not accumulate tracer particles and leaves a clear trail free of tracers due to the flows that push tracers away from the ends of its legs.

To better quantify this change in swimming direction, we sampled individual particle velocities at different fuel concentrations and identified the transition region where the reversal takes place, see Fig. 3.3 (see Appendix for examples of particle trajectories). We mark the change in direction through a change in sign. Catalytic-side leading particles have a negative velocity while inert-side leading particles have a positive velocity. The speeds are in line with typical speeds reported for active spheres[24], crescents[15], microtori[16] and rods[25] of similar size and with a catalytic platinum patch. For all shapes where we observe two swimming directions the change in propulsion direction appears around 4-5 wt% H_2O_2 followed by a transition region in which both directions are observed in significant amounts, i.e. we report both species when the minority species accounts for at least 30%

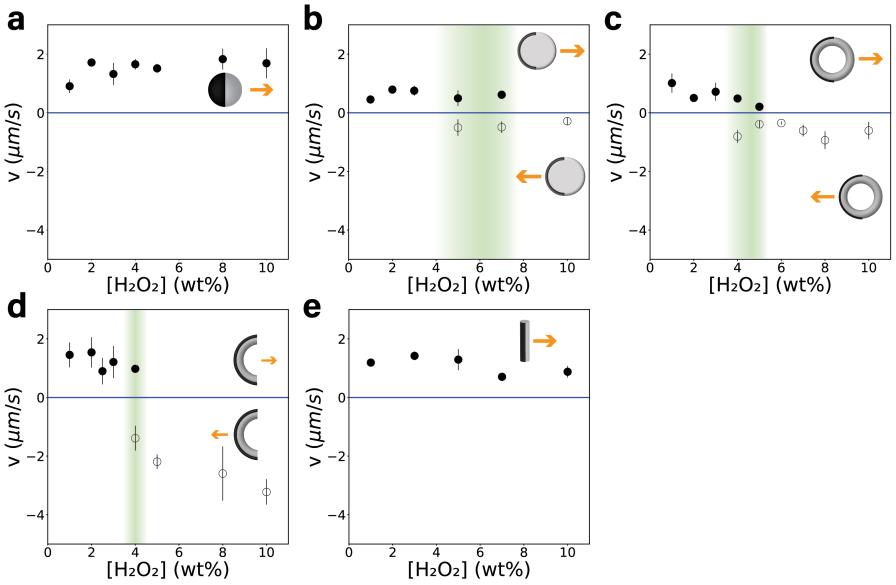

Figure 3.3: Influence of the fuel concentration. Particle velocities plotted against fuel concentrations for spheres (a), discs (b), tori (c), crescents (d) and rods (e). The transition region from positive velocity (inert-side leading) to negative velocity (catalytic-side leading) is highlighted in green. Plotted points are median values and error bars represent first and third quartiles.

of the particles. This transition region becomes narrower the more the shape deviates from a sphere but side-propelling straight rods swim again inert side-forward at all fuel concentrations. For discs this region stretches over a concentration range between 5-7 wt% H_2O_2 while for tori it narrows down to a concentration of 4-5 wt%. For crescents the transition occurs sharply at 4 wt%. Moreover, the results presented in Fig. 3.3a suggest that the chemical decomposition rate is fixed as only a negligible correlation between the propulsion speed and the peroxide concentration can be observed. These results suggests that the swimmer's direction of motion is not influenced by the material alone but by its shape as well as by the H_2O_2 concentration.

Effect of the Material Composition of the Inert and Catalytic Sites.

As the cap material is known to influence the swimming direction of active spheres[14] and microtori[16], we proceed to test whether the material of the inert and catalytic part contribute to the appearance of the direction reversal as well. We start by investigating the effect of the material composition of the catalytic site. The catalytic side of the swimmers experiments presented in Figures 3.1-3.3 consisted of Pt/Pd with traces of platinum oxide

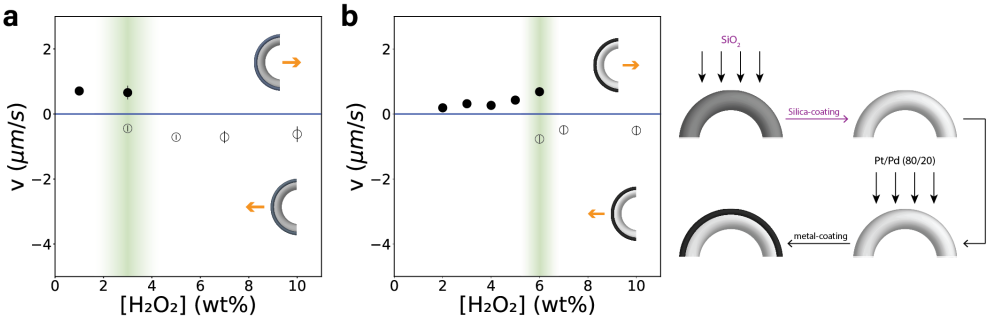

Figure 3.4: Influence of the inert and catalytic surface material. Dependence of the particle velocity on the fuel concentration for (a) crescents with pure Pt/Pd coating, without PtO contamination, and (b) silica-coated crescents. The transition region, in green, from positive velocity (inert-side leading) to negative velocity (catalytic-side leading) shifts to lower fuel concentrations when the composition of the catalytic cap-material changes (absence of oxide). When the exposed inert surface is composed of silica the transition region shifts to higher fuel concentrations.

(PtO), see Appendix. We note that while the presence or absence of PtO has been shown to change the swimming direction of SiO_2-Pt Janus particles[8], this cannot explain the direction reversal reported here, which was observed for the same particle at different fuel conditions. However, this presents an opportunity to use pure Pt/Pd for the catalytic cap, which is then a different but closely related material. When preparing swimmers with pure Pt/Pd caps, both directions of motions at different fuel concentrations are still observed: the inert-side leading (positive velocity) at low fuel and the catalytic-side leading (negative velocity) at high fuel (Fig. 3.4a). The transition region from positive to negative velocity shifts to lower H_2O_2 concentrations for the Pt/Pd coating (Fig. 3.4a). Moreover, Pt/Pd-coated spheres do not exhibit reversals, similar to Pt-only spheres, excluding that Pd causes the reversal of the propulsion direction. These experiments thus demonstrate that the type of metal affects the precise conditions at which direction reversal occurs but not whether it occurs at all.

To complete the picture, we varied the material composition of the inert surface of crescent-shaped microswimmers. For this, particles were fully coated with silica (SiO_2) using a high vacuum sputter coater with custom modifications, before applying the catalytic film on the convex side of the crescent, see Materials and Methods section and Appendix. After dispersion in H_2O_2, we observe both swimming directions for SiO_2-modified crescents similar to the behavior of the IP-Dip particles. The transition region shifts to higher fuel concentrations and appears at a somewhat higher H_2O_2 concentrations of 6wt% H_2O_2, see Fig 3.4b. Moreover, the average propulsion speed of SiO_2-coated particles was found to

be significantly lower across all fuel concentrations, see Fig 3.4b. This can be understood from the more hydrophilic surface properties of silica compared to IP-DIP, which is known to cause lower propulsion speeds, especially for larger sized particles[7]. IP-DIP has a water contact angle (CA) of $\sim 50^\circ$ (see Appendix), whereas bare silica particles the CA is less than 10° [26]. We thus find that the direction reversal of anisotropic particles persists for different surface properties, precisely for exchanging Pt/Pd/PtO with Pt/Pd and IP-DIP with silica.

We finally tested whether exposure to high fuel conditions might change the surface chemistry in an irreversible manner by exposing crescent-shaped particle first to high hydrogen peroxide concentrations before testing their swimming and direction reversal at lower fuel concentration. No change was observed, indicating the absence of any lasting changes in the surface chemistry.

Finally, we note that the swimming velocity itself is not the decisive parameter that can explain direction reversal. The presence of PtO enhances the velocity of the swimmer and delays the onset of the reversal to higher H_2O_2 concentrations. In contrast, a more hydrophilic inert surface reduces the crescent velocity while also shifting the transition region to higher H_2O_2 concentrations. There is hence no simple correlation between the particle speed and the fuel concentration at which direction reversal occurs.

Effect of the Particle Orientation At fuel concentration close to the transition region, we occasionally observe SiO_2-coated crescents to flip, sometimes combined with a change in swimming direction (see image sequence Fig 3.14 in Appendix and Supplementary Videos 13-14). Similarly, occasional flipping has also been observed for smaller 7 μm crescent which were not silica coated (see Appendix Fig. S8). The flipping suggests that the orientation of SiO_2-coated crescents in the xy-plane is not fully stable. Active spheres, in contrast, show a strong coupling of their symmetry-broken axis to the substrate leading to a small and stable tilt towards the substrate that slightly increases with fuel concentration[27]. This has been proposed to arise from a balance between an activity-induced torque (T_a) and a gravitational torque stemming from the mass anisotropy due to the metal half-coating (T_g), but might also be a sign of osmotic surface flows. We find, however, that the unstable orientation of the particles is not the origin of the direction-reversal mechanism, but rather a consequence of the different propulsion directions, see Appendix for details.

Combination of pH-dependent surface properties and the particle geometry After

having investigated possible intrinsic direction-reversing effects related to the active particle itself—such as material composition, orientation, or size—we now turn to changes induced by external experimental conditions, specifically variations in fuel concentration. For discs, tori and crescents the directionality of the particle velocity depends on the H_2O_2 concentration and starts reversing at about 4 wt% fuel (cf. Fig. 3.3). As H_2O_2 is a weak acid, the pH of the solution decreases with increasing H_2O_2 concentration for all fuel solutions (Fig. 3.5a). We note that the pH changes most rapidly in the concentration range where discs, tori and crescents propel inert-side forward.

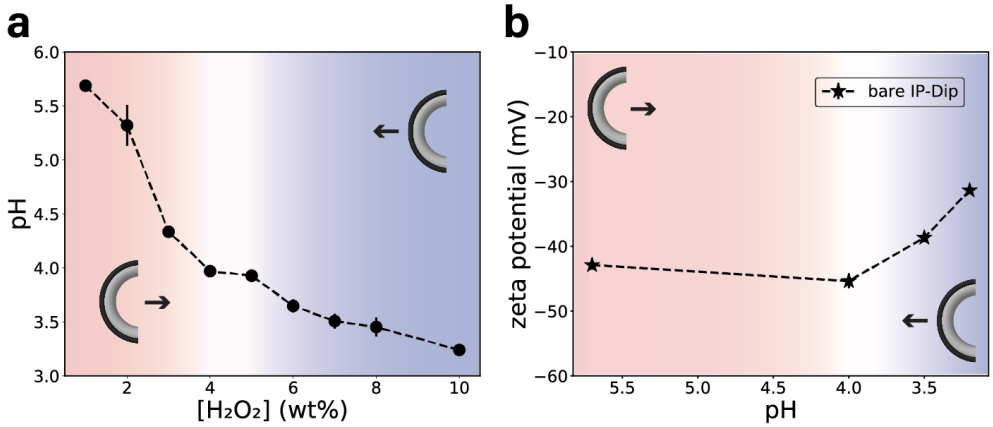

Figure 3.5: Fuel concentration dependence of pH and zetapotential. (a) H_2O_2 concentration of the fuel solutions plotted against pH. The approximate concentration range where discs, tori and crescents propel inert-side forward is highlighted in red. The blue range corresponds to fuel concentrations where catalytic-side leading propulsion was observed. The transition region where both motion directions are observed is highlighted in white. Data points were connected by a dashed line to guide the eye. (b) The surface zeta potential increases with decreasing pH but always remains negative for bare IP-Dip particles.

The change in pH directly affects the surface properties of both catalytic and inert sides of the particles. The zeta potential of platinum has been reported to decrease from -10 mV at pH 3.2 to -55 mV at pH 5.7[?] , indicating an increasingly negative surface charge with rising pH. In contrast, for 3D-printed IP-Dip particles, the zeta potential becomes less negative with increasing fuel concentration, changing from -42.9 mV to -31.6 mV (see Fig. 3.5b). Within the pH range relevant to our experiments, the zeta potential of the catalytic side thus becomes more negative than that of the inert side. As the fuel concentration increases and the pH decreases, the relative magnitude of the zeta potentials, i.e $\zeta_{inert}/\zeta_{catalytic}$

correspondingly decreases while remaining close to unity. Literature reports suggest that a similar trend holds for silica–Pt systems[28,29].

A relative zeta potential change implies a relative change in phoretic mobility which, besides the shape, has been proposed to be a key parameter in determining the propulsion direction[21]. Using numerical simulations within a self-diffusiophoretic framework, Michelin and Lauga[21] showed that for prolate particles with aspect ratios greater than five and mobility ratios of order unity, even small changes in the mobility ratio can induce a reversal of the swimming direction. In contrast, for spheres and oblate particles, a negative mobility ratio—corresponding to zeta potentials of opposite sign on the two Janus halves is required to achieve direction inversion. The origin of the different behavior of the shapes are that anisotropic shapes lead to solute confinement and hence to local concentration differences in the fuel and product. Further, the authors showed that for three-dimensional particles with broken symmetry, the dominant contribution arises from the two-dimensional projection of their shape with the highest solute concentration.

Interpreting our experimental results in light of their calculations, we can straightforwardly explain why spherical particles should not revert their direction. The reason is that the ζ potential ratio does not change sign. Similarly, rod-like particles moving along their short axis have the highest solute concentration projected out onto their spherical cross-section and hence can be approximately treated as spheres. Thus, they should likewise not revert.

For crescents, tori and disks, the dominant projection yields a disk, a shape that is close to a prolate object, as studied by Michelin and Lauga[21]. For the zetapotential and hence phoretic mobility ratios measured in our experiments, these results predict a pronounced sensitivity to surface properties for discs—and by analogy also for tori and crescents— around a relative zetapotential of order 1 in full agreement with our observations. We note that zetapotential measurements of silica coated IP-dip particles were not conclusive. Our experiments therefore suggest that the relative electrophoretic mobilities of the two halves of the Janus particle set the direction of propulsion, and that this reversal is strongly dependent on the particle geometry.

Substrate-induced Solute Confinement While the work of Michelin and Lauga[21] can explain our results and allows interpreting them in terms of shape induced concentration gradients together with a pH induced change in surface properties, these predictions

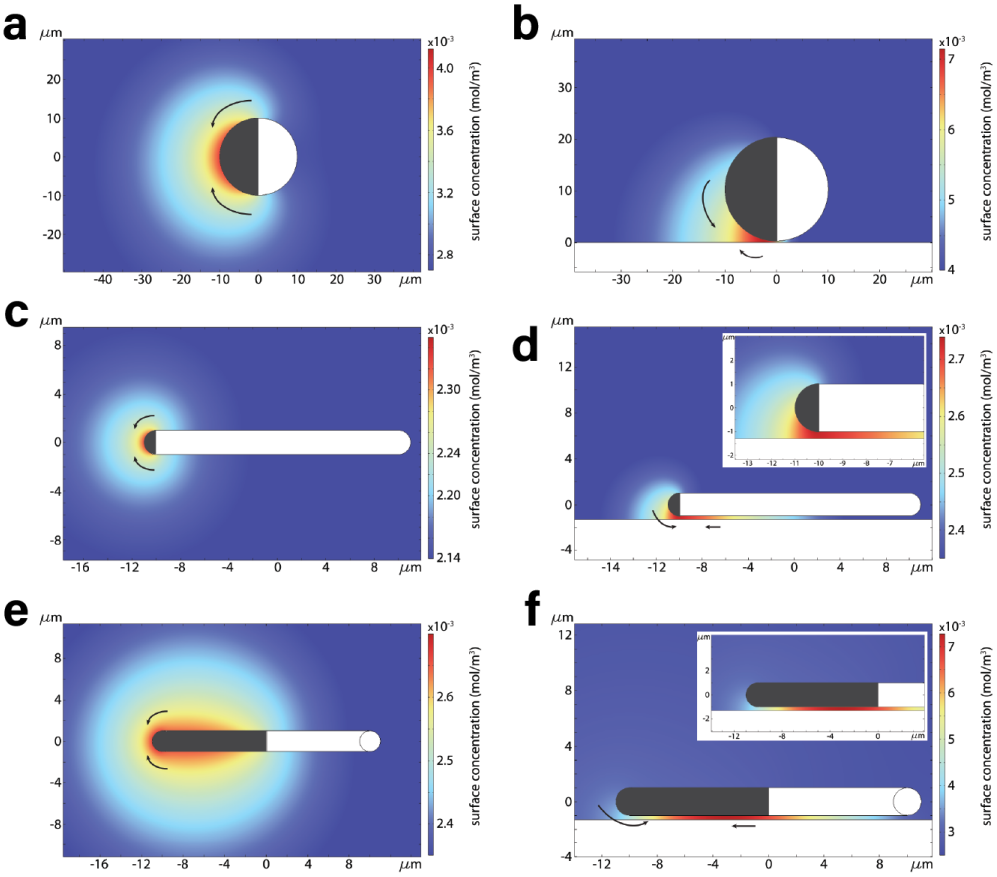

Figure 3.6: COMSOL simulation of the spatial distribution of the chemical product H^+ around Janus particles of different shapes. Panels (a), (c), and (e) show the distribution in the bulk, while panels (b), (d), and (f) show the distribution near a substrate. (a)–(b) represent a Janus sphere with a hemispherical cap (black) producing H^+ at a flux of J_{0,H^+}. (c)–(d) show a Janus disk where only the curved edge (black) emits H^+ with a flux of J_{0,H^+}. (e)–(f) depict a Janus disk where the curved edge produces H^+ with a flux of J_{0,H^+} and the flat half-side emits at a reduced flux of $\frac{1}{3}J_{0,H^+}$, mimicking the inhomogeneous coating of the active layer. The surface slip flows are schematically indicated with black arrows. See Materials and Methods for further details.

have been made for particles in solution. In our experiments, however, a substrate is nearby, which might further influence the occurrence of the direction reversal through osmotic surface flows and the solute concentration profiles.

To test for significant influence of osmotic flows, we performed experiments with commer-

cially available cells with a highly hydrophilic surface (μm-slide, Ibidi (Cat.No:80326)) as well as glass slides. Direction reversal was found to occur on both surfaces, indicating that while details might change, the effect persists.

To test this, we use COMSOL simulations to obtain the spatial distribution of the chemical product around Janus particles with a spherical and elongated shape. In the simulation, protons (H^+) are emitted from the active side with a constant flux $J_{0,H^+} = 1 \times 10^{-6}\,\mathrm{mol\,m^{-2}\,s^{-1}}$ at the active sides or $\frac{1}{3}J_{0,H^+}$ at the flat side. Transport is assumed to occur by diffusion, with a diffusion coefficient $D_{H^+} = 9.31 \times 10^{-9}\,\mathrm{m^2\,s^{-1}}$ (cf. Materials and Methods section for more details). We here again consider two-dimensional projections of the particles as a means to capture the confinements induced by their 3D shape. In this representation, tori, crescents, and disks yield again indistinguishable 2D projections, while rods and spheres likewise share the same projection.

For a half-coated Janus sphere or side-propelling rod, the solute concentration gradient in the 2D projection typically has its maximum at the active pole (Fig. 3.6a), similar to the findings in[21]. Introducing a nearby wall causes this maximum to shift closer to the wall, see Fig. 3.6b. In the case of an elongated particle with a catalytic cap covering only the rounded edge, the same confinement effect can push the concentration maximum underneath the particle, toward the center of the confined area (Fig. 3.6c and d). This shift becomes even more pronounced when the catalytic coating extends beyond the edge and partially covers both the top and bottom surfaces of the particle, see Fig. 3.6e and f. Since concentration gradients induce fluid flows from low to high concentration, we expect these confinement-induced changes to the concentration profile to enhance the direction reversal of the surface slip flows, and consequently the reversal in the propulsion direction.

Interestingly, the substrate-induced confinement may explain the different widths of the transition regions between forward and backward swimming. The transition region is the broadest for discs, narrower for microtori and becomes very sharp for crescents, in line with the increasingly smaller confinement area that their particle shape induces. Moreover, we expect a positive feedback mechanism once the swimmer moves into a certain direction: motion towards the cap would drag the solute gradient further underneath the particle while a propulsion away from the cap would drag it closer to the edge of the particle. This could explain the presence of particles with both propulsion directions in the transition region that we have observed as well as the stability of the particles direction of motion when placed in a linear concentration gradient, see Appendix.

3.3 Conclusion

In summary, we report a reversal of the propulsion direction with increasing fuel concentration for catalytically active anisotropic Janus colloids half-coated with Pt/Pd and suspended in aqueous H_2O_2 solution. This direction reversal is shape dependent and can be observed for discs, tori, and bend rods (crescents), but not for spheres and straight rods propelling along their short axis. At low fuel concentrations, particles propel with their inert-side forward while at higher fuel concentrations the swimming direction changes and particles move catalytic-side forward. In contrast, spheres and rods always move inert-side leading independent of the H_2O_2 concentration. We find that the fuel concentration at which the directionality of the particle velocity switches from inert-side leading to catalytic-side leading, is influenced by the material of the microswimmer and by the presence of oxide-contamination in the catalytic Pt-cap. An overview of our findings is shown in Fig. 3.7.

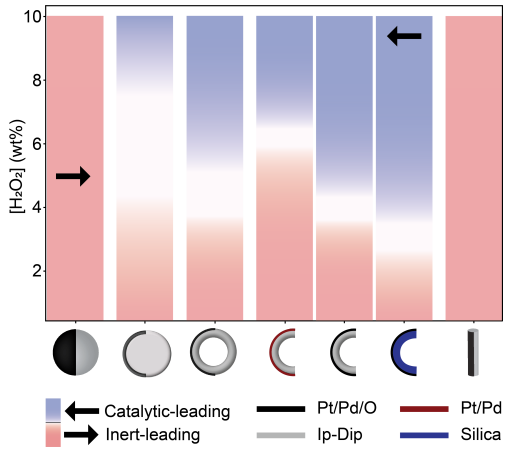

Figure 3.7: Overview of the different propulsion directions for all particles presented in this work The swimming direction depends on the particle geometry as well as on the zeta potential ratio of inert and catalytic material.

We showed that the propulsion direction is governed by combined effects of pH-dependent surface properties, particle geometry, and substrate-induced solute confinement. Increasing H_2O_2 concentration lowers the pH, which reduces the surface zeta potentials of both Janus sides and leads to a change in the relative zeta potential ratio. This behavior correlates with a reversal in swimming direction for discs, tori, and crescents but not for spheres or rods. This directly confirms the predictions of Michelin and Lauga[21] that, for anisotropic prolate-like geometries and mobility ratios close to one, small changes

in surface mobility can invert propulsion direction, whereas symmetric or oblate shapes require opposite-sign mobilities. COMSOL simulations moreover reveal that the nearby substrate further confines reaction products and reshapes concentration gradients in a geometry-dependent manner, which enhances the effect. The width of the transition region and the observed stability of swimming direction can be rationalized by shape-dependent confinement and positive feedback between motion and solute gradients, demonstrating that propulsion direction emerges from the interplay of surface chemistry, geometry, and substrate-induced confinement.

3.4 Methods

Reagents

Fused silica substrates and IP-Dip photoresist were purchased from Nanoscribe GmbH. The platinum-palladium target (Pt/Pd 80:20) was acquired from Micro to Nano. Propylene glycol methylether acrylate (PGMEA, ReagentPlus $\geq$ 99.5%) was purchased from Sigma Aldrich and isopropanol (IPA) was obtained from VWR chemicals. Hydrogen peroxide (H_2O_2, 35 wt% solution in water, stabilized) was purchased from Acros Organics. Water was filtered with a MilliQ MilliPore system (resistivity $\geq$ 18 MΩ.cm). Unless otherwise noted, all chemicals were of analytical or reagent grade purity and were used as received from commercial sources.

Particle Fabrication

All colloidal particles were 3D printed on a Nanoscribe Photonic Professional GT micro-printer equipped with a 63x oil-immersion objective (Zeiss, NA = 1.4). We have described the printing routine in details in our previous work[22]. The spheres have a diameter of 7 μm. discs and tori were designed with a diameter of 10 μm and a thickness of 2 μm. The crescent structure corresponds to a half-tori with identical shape parameters. The rods are 10 μm long and 2 μm thick. Discs, tori, and crescents were printed standing up while rods were printed lying down on the substrate. All particles were printed on fused-silica substrates using IP-Dip as photoresist. The prints were developed in PGMEA for 30 min, followed by 2 min in IPA. Particles were made active by half coating them with a 5nm thick platinum-palladium film (Pt/Pd 80:20) using a Cressington 208HR sputter coater and argon as the inert gas in the sputtering chamber. Only afterwards the Janus microstructures were removed from the substrate by sonication in water, as described in ref.[15].

For active silica-coated particles a 50 nm thick silica film was applied after developing but before sputter coating with platinum-palladium. For this, a high vacuum Leybold-Heraeus Z400 sputter-coater with custom modifications was used to obtain a coating of all exposed particle surfaces. The target was positioned close to the sample and sputtering was performed at $\approx 10^{-5}$ mbar (Ar @ 54 sccm, Direct Current Electrde Positive (DCP): 1kV) which yields a robust layer that covers most of the particle.

Propulsion of Active Particles

Pt-coated colloidal particles were suspended in freshly prepared aqueous hydrogen peroxide solution and placed in a sample holder ($\varnothing = 8$ mm) with an untreated borosilicate glass coverslip (VWR, 25 mm, No. 1) as substrate. To prevent evaporation, the sample was covered with a second coverslip. The self-propulsion of these microswimmers arises from the catalytic decomposition of H_2O_2 at the Pt/Pd cap[1,3].

Data Acquisition and Analysis

The active particles were observed under a Nikon Eclipse Ti-E bright-field light microscope with a Plan Apo λ 20x long working distance objective (NA = 0.75). 30s long videos with a frame rate of 20 fps were recorded to obtain the average particle velocity for all individual shapes.

The particles were tracked by applying the Canny Edge detection algorithm to each frame to generate a mask from which the particle center of mass was obtained. Individual particle velocities v and diffusion coefficients $\mathcal{D}$ were determined by fitting the mean squared displacements (MSDs) with $\Delta r^2 = 4\mathcal{D}\Delta t + v^2\Delta t^2$ up to lag times much smaller than the rotational timescale for a sphere ($1.25\ s \ll 50\ s$). We here use the fit equation originally developed for spherical active particles[1,30] as an approximation also for non-spherical particles. This yielded consistent and reliable results, albeit without subpixel resolution.

z-Stack in Confocal Mode and crescents in a tracer particle bath

Z-stacked confocal images were captured with a Nikon Eclipse Ti microscope equipped with an A1R confocal scanning head and a 60× (NA = 1.2) water immersion objective. A z-stack image sequence consisted of multiple images recorded at different focal heights. A MCL Nano-Drive piezo was used to acquire high speed z-stack images for active 10 µm sized crescents in 1wt% and 10wt% H_2O_2 as well as for a 7 µm crescent in 1wt% H_2O_2. The scanning was executed from bottom to top with a scan time of 0.6 sec per z-stack image.

To visualize the flow profiles for different propulsion directions, we introduce fluorescent 1.77-µm-diameter TPM tracer particles[23] and track their behavior in confocal mode with a 100x (NA = 1.3) oil immersion objective near inert side moving or catalytic side moving crescents.

Zeta-potential Measurements

Zeta potential measurements were performed with a Malvern Zetasizer Nano ZS which determines the electrophoretic mobility of colloidal particles moving toward an electrode of opposite charge using a technique called Laser doppler velocimetry. The zeta potential is obtained from the electrophoretic mobility by applying the Henry equation, which is incorporated in the software of the apparatus. Spherical, 2 μm sized, 3D printed particles were used for zeta-potential measurements in aqueous solutions with the pH being adjusted using HCl. The pH of all solutions was measured with a pH meter from VWR. We also attempted to measure the zetapotential of IPdip 3D printed particles sputtercoated wtih silica and platinum, similar to the experimental fabrication. However, sputtercoating leaves the patch of the particles surface in contact with the substrate uncoated. The obtained zetapotential values were dominated by this uncoated patch of IPdip, as they agreed within the error with the values measured for pure IPdip particles and diverged clearly from literature values.

COMSOL simulations

The species distribution around the particles is simulated using COMSOL Multiphysics with a two-dimensional model incorporating the Transport of Diluted Species (tds) module. We simulate particles with both flat disk and spherical geometries, located either in bulk solution or near a solid substrate (300 nm above the substrate). The simulation domain is a square region of water measuring $200\,\mu\text{m} \times 200\,\mu\text{m}$. As a demonstration, we used protons (H^+) as diffusing species. Only diffusion is considered for simplification. The diffusion coefficient of H^+ is set to $D = 9.31 \times 10^{-9}\,\text{m}^2/\text{s}$, with an initial concentration of $2 \times 10^{-3}\,\text{mol}/\text{m}^3$, based on the pH of 5.7 resulting from the dissolution of CO_2 in Milli-Q water. A flux of magnitude $J_{0,\text{H}^+} = 1 \times 10^{-6}\,\text{mol}/(\text{m}^2 \cdot \text{s})$ and is applied to the active sides of the particles and $\frac{1}{3}J_{0,\text{H}^+}$ to the flat sides with reduced activity. The inert sides of the particles and the substrate are assigned a no-flux boundary condition. The outer boundaries of the water domain are maintained at the initial concentration, effectively mimicking an infinite bulk environment. A super fine mesh is applied to regions near the

particles and substrate, built on top of a free triangular mesh.

3.5 Appendix

3.5.1 Particle design

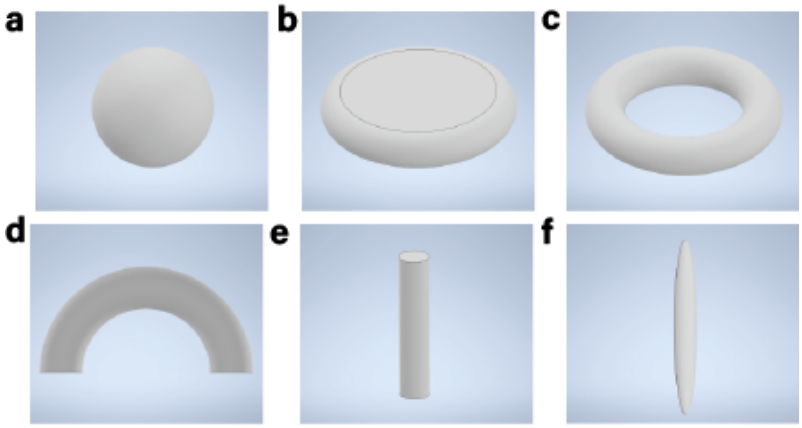

Figure 3.8: CAD design for 7 µm spheres, 10 µm disks, 10 µm tori, 10 µm crescents, 10 µm rods and 10 µm ellipsoid.

3.5.2 SEM images of crescent-shaped particles

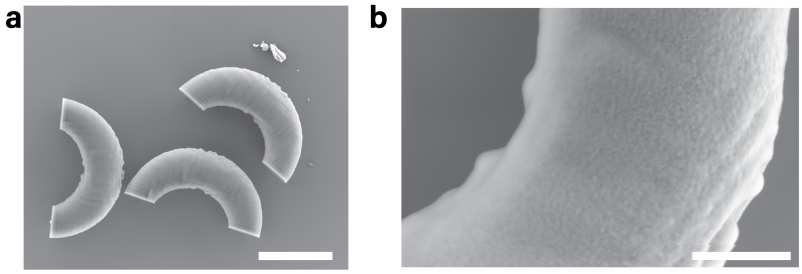

Figure 3.9: SEM micrographs of Pt/Pd coated crescent-shaped particles. The scale bars are a) 5 μm, b) 1 μm.

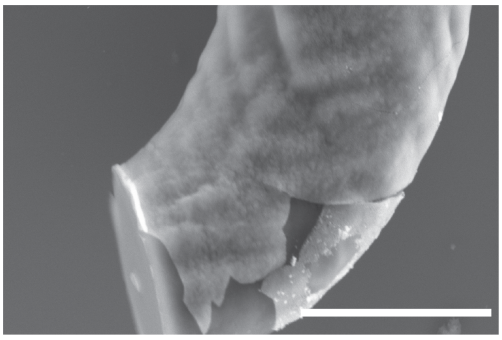

Figure 3.10: SEM image of a silica-coated crescent-shaped colloids used in this work The silica coating covers also the inner concave part of the crescent and in this example is cracked at the bottom of the leg. The surface of the crescent-feet that was in contact with the substrate during the coating process is not covered. The scale bar is 2 μm.

3.5.3 Particle velocities plotted against fuel concentrations for concave-side coated crescents

Concave-side coated crescents show direction reversal at increasing hydrogen peroxide concentrations, see Fig. 3.11. The particles often show spinning and circular motion, most likely because the sputter-coating process deposits metal not only in the concave side, but also on the crescent 'feet'.

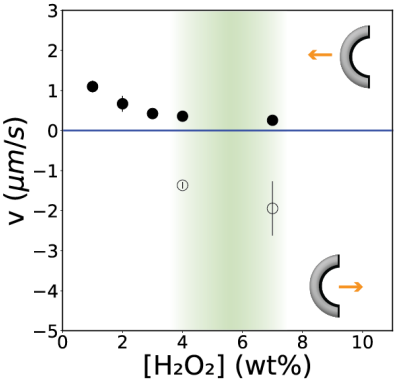

Figure 3.11: Both swimming directions are observed depending on the fuel concentration. The transition region from positive velocity (inert-side leading) to negative velocity (catalytic-side leading) is highlighted in green. Plotted points are median values and error bars represent first and third quartiles.

3.5.4 Centered particle trajectories for top-coated crescents at different fuel concentrations

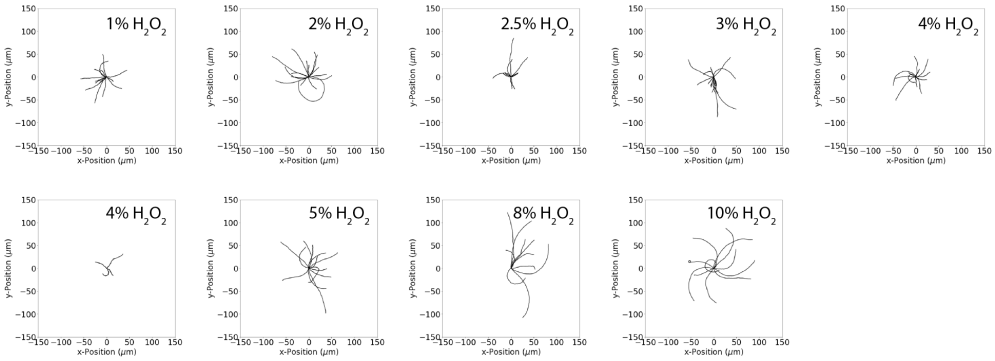

Figure 3.12: 30 sec trajectories for crescents coated on their curved side at different H_2O_2 concentrations. Active crescents are swimming inert-side leading (top row) and catalytic-side leading (bottom row) depending on the fuel concentration. The direction reversal occurs at 4 wt% H_2O_2 and both swimming directions are observed at this transition concentration. The average particle velocity extracted from this data can be found in Fig.3 d.

3.5.5 Diffusion constants at different fuel concentrations for all shapes

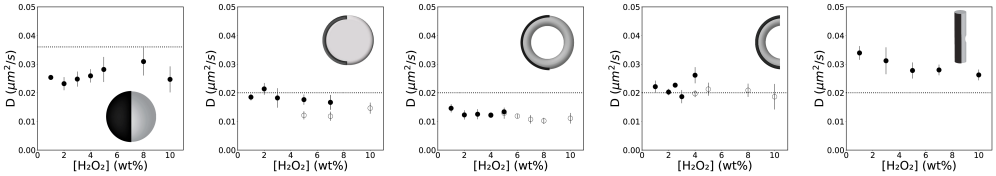

Figure 3.13: Diffusion constant D for 7 μm spheres, 10 μm disks, 10 μm tori, 10 μm crescents and 10 μm rods in different fuel concentrations. The diffusion constants were extracted from fitting the MSD. The dotted line indicates the expectation value for an equally sized sphere close to the substrate with a radius of 3.5 or 5 μm, respectively[24]. Plotted points are median values and error bars represent first and third quartiles. Black markers correspond to inert-side leading particles and white markers correspond to catalytic-side leading particles

3.5.6 Active crescents in fuel concentration gradients

To examine the influence of a fuel concentration drop over time due to fuel decomposition, we exposed our active crescents to a stable linear concentration gradient (1wt% - 7wt%

H_2O_2) generated in a µm-slide for chemotaxis from ibidi (Cat.No:80326). These slides are coated with a highly hydrophilic coating, allowing furthermore to test the persistence of the direction reversal for different surface boundary conditions. After setting up the linear gradient, the region occurring at 4 wt% H_2O_2 for crescents corresponds to a region with a width equivalent to approximately 9 crescent lengths. We find that crescent-shaped particles still showed different directions of motion in the respective parts of the gradient, however, more crescents displayed circular trajectories compared to samples exposed to a single, uniform concentration.

Surprisingly, we could not observe the particles reverse their direction when crossing the concentration region where reversal was observed in homogeneous samples, see Supplementary Videos 16. We believe that this is because of a self-stabilizing effect. That is when the particles move, their concentration maximum shifts with regard to the particle thereby stabilizing the initial propulsion direction. Only one crescent that began its motion in the transition region was observed to reverse its propulsion direction, switching from polymer-side-leading to catalytic-side-leading. This change in direction occurred via a rotational reorientation. However, the transition did not coincide with the corresponding change in fuel concentration: the crescent continued to propel with its catalytic side forward even within the low-concentration region.

3.5.7 Flip of self-propelled crescents

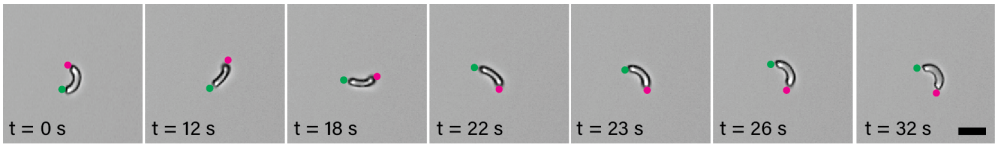

Figure 3.14: Flip of a SiO_2-coated crescent. At a fuel concentrations corresponding to the transition region, we occasionally observe particles that flip. This can come with a change in swimming direction but this is not always the case. Here the crescent moves inert-side forward before and after the flip. The two crescent feet are color-coded to guide the eye and help the reader to see the flip. The scale bar is 10 µm.

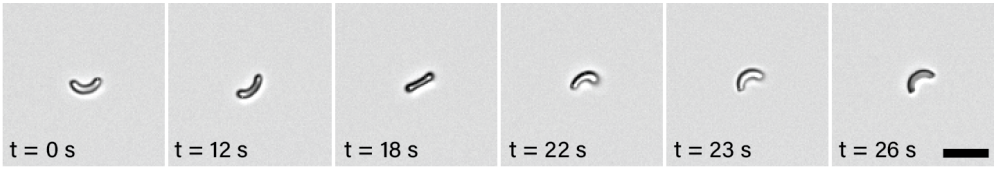

Figure 3.15: Flip of a 7 µm sized crescent. Smaller crescents are also occasionally observed to flip at fuel concentrations close to the transition region. However, a change in swimming direction was never observed for flipping 7 µm crescents. The scale bar is 10 µm.

3.5.8 Effect of the Particle Orientation

While tilting of spherical - and likewise our rod-shaped - particles along their propulsion direction can be executed without any steric constraints and does not impose any changes to the distances between the particle surface and the substrate (see Fig. 3.16a), this is different for anisotropic particles that do not posses a spherically symmetric cross-section along the propulsion direction (see Fig. 3.16b). For discs, tori or bend rods (crescents), tilting would induce an additional symmetry breaking in the propulsion direction. Moreover, the distance with respect to the substrate varies along those particles when tilted, and also changes with different tilt angles α, see Fig. 3.16b.

To determine whether our crescent-shaped microswimmers assume a tilted orientation, we use confocal microscopy and perform a z-stack imaging of the moving particles in 1wt% and 10wt% H_2O_2, respectively. We note that taking a stack of images in the z-direction might cause a distortion of the image because the moving particle displaces in the x-direction between the top and bottom images of the stack. From the particle speed we estimate this x-displacement to be about 500nm, or 10% of the particle size in this direction.

For particles with 10μm cross-sectional length, no significant tilt can be observed in either fuel concentration, although the lower boundary of the particle at 10wt% H_2O_2 suggests a small upward tilt in the moving direction, see Fig. 3.16c (right). When the cross-sectional length of the crescent is reduced to 7 µm, we occasionally observe a downward tilt of the crescent legs with respect to the substrate in 1wt% H_2O_2 (Fig. 3.16d, left). In contrast to Janus spheres which exhibit strong orientational locking, the orientation of the smaller crescents is not stable and fluctuates between a parallel and a tilted position (see Fig. 3.18). The downward tilt of the legs in the moving direction is in line with the tilt direction of active spheres[27], and not an imaging artifact as the distortion of the z-stacked image due to the motion of the swimmer is opposed to the observed tilt. Occasionally, we

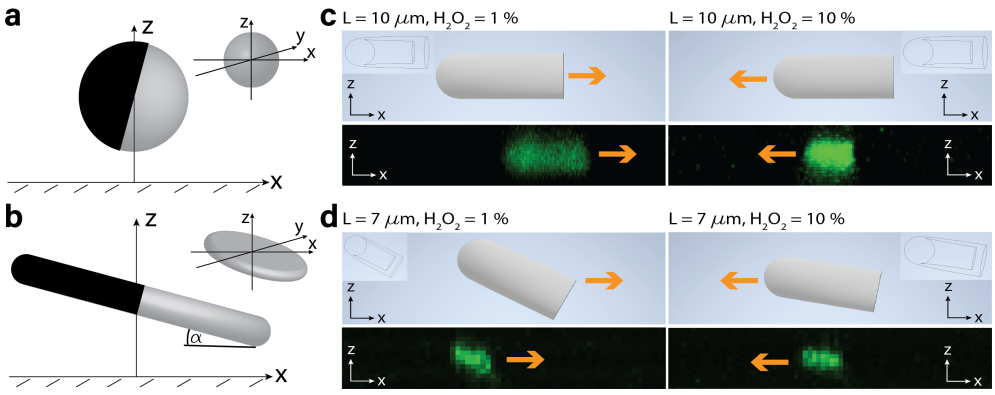

Figure 3.16: Influence of a tilted particle orientation. (a) A sphere tilted with respect to the substrate does not change the distances between the particle and the substrate. This is also true for rod-shaped particles propelling with their velocity director pointing perpendicular to their long axis as their cross-sectional shape in the zx-plane is identical to that of the sphere. (b) A tilted orientation in anisotropic shapes like discs, tori and crescents leads to an asymmetric confinement between the particle and the wall. This is exemplarily shown for the simplest of these shapes, a disc. (c) Projection of a confocal z-stack in the zx-plane and schematic illustrating the crescent orientation, for 10 μm sized crescents in 1wt% (left) and 10wt% (right) H_2O_2, respectively. No significant tilt can be observed for 10 μm crescents. (d) Schematic and z-stack projection for 7 μm crescents in 1wt% (left) and 10wt% (right) H_2O_2. In 1wt% H_2O_2 smaller crescents occasionally adopt a tilted orientation. In 10wt% H_2O_2 the tilt is much less pronounced.

also observe a tilt in the direction perpendicular to the propulsion, with the legs not being equally close to the substrate (see Fig. 3.19). When suspended in 10wt% H_2O_2, 7 μm crescents show a less pronounced tilt which is now away from the substrate in the moving direction, see Fig. 3.16d (right).

We attribute the difference in behavior between smaller and larger crescents to the effect of their size on the competition between activity-induced torques and the gravitational torques required to lift and tilt the anisotropic particle. In the absence of activity, Janus-crescents adopt a flat, parallel orientation relative to the substrate. For an active torque to induce a tilt not only must the mass asymmetry caused by the metal coating be overcome, but the particle also needs to be lifted away from the substrate to be able to tilt. The active torque achieves this for the smaller and lighter crescents reorienting them such that the director points into the substrate, but not for the larger heavier ones. At high fuel concentrations, the particles propel with their convex side forward, generating a propulsion force directed away from the legs. This reverses the direction of the activity-induced torque and consequently reduces the tilt.

Further evidence for the presence of a tilt stems from an analysis of the diffusion coefficient (see Fig. 3.13 for diffusion constants of other shapes). The stronger tilt orientation of inert-side leading 7 µm crescents should cause the center of mass of the particle to shift further away from the substrate. This increased height should be reflected in a higher diffusion coefficient D[24] and particle speed due to reduced hydrodynamic interactions with the substrate. Before the direction reversal, the average diffusion constant of 7 µm crescents is indeed significantly larger than after, suggesting that the particle has assumed a flatter orientation after direction reversal, see Fig. 3.17a. A larger height between the particle and the substrate also means that smaller particles experience a weaker hydrodynamic coupling with the wall which is expected to stabilize their orientation. This is in line with our observation that at fuel concentrations close to the transition region, some 7 µm crescents have also been observed to flip (see Fig. 3.15 and Supplementary Videos 15), which suggests an orientational instability.

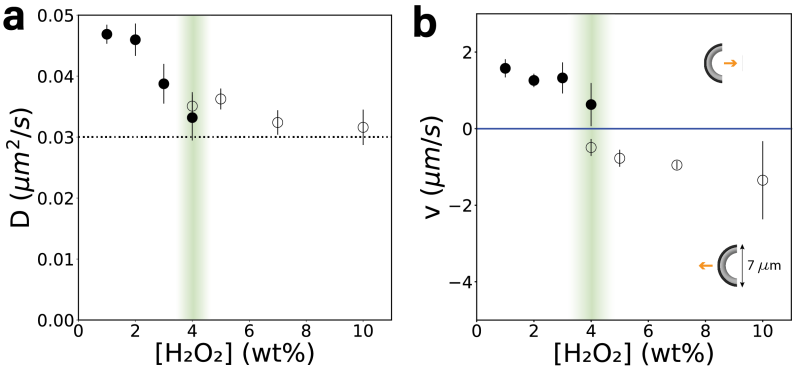

Figure 3.17: Diffusion constant and particle velocity for 7 µm crescents in different fuel concentrations. (a) Height-dependent diffusion constant D for 7 µm crescents in different fuel concentrations. A stronger tilt for inert-side leading crescents in lower fuel reflects in a higher D. The dotted line indicates the expectation value for an equally sized sphere with a radius of 3.5 µm close to the substrate[24]. (b) Dependence of the average particle velocity on the fuel concentration. The transition region, in green, is unaffected by a change in particle size.

We further note that the average particle velocities of 7μm crescents at low H_2O_2 concentrations is comparable to the values obtained for 10 µm crescents and the location of the transition region is unaffected by a change in particle size (cf. main text Fig. 3.3d). Beyond the transition the average particle velocity increases with increasing fuel concentration but does not reach the high values observed for 10 µm crescents (cf. main text Fig. 3.3d).

Based on these findings, we conclude that for 7 µm crescents the propulsion direction results in different particle orientations with respect to the substrate and that the swimming direction reverses sharply at 4 wt%. Since larger crescents also show direction reversal with the same sharp transition region but are not significantly tilted with respect to the substrate, we conclude that a change in particle orientation is an effect of different propulsion directions and not the cause of it.

3.5.9 Confocal z-stack imaging of 7 µm crescents

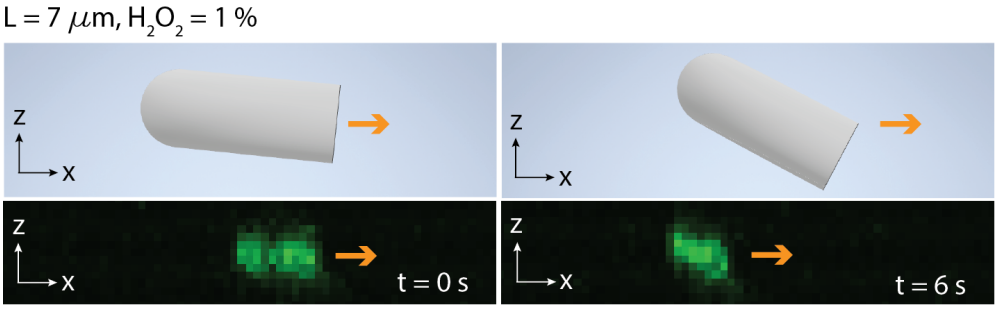

Figure 3.18: Orientation of a 7 µm crescents in 1wt% H_2O_2, side view. Projection of a confocal z-stack in the zx-plane and schematic illustrating the crescent orientation. The orientation of our smaller crescents is not stable and we see it fluctuate between a parallel (left) and a tilted (right, taken from main text) position.

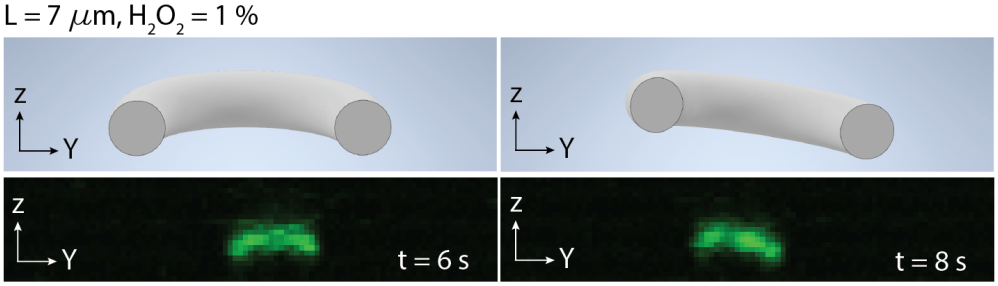

Figure 3.19: Orientation of a 7 µm crescents in 1wt% H_2O_2, front view. Projection of a confocal z-stack in the zy-plane and schematic illustrating the crescent orientation. An occasional tilt where both legs are not equally close to the substrate is also observed for smaller crescents in low fuel.

3.5.10 EDX measurements

Energy-dispersive X-ray spectroscopy was used to identify the presence of oxide (PtO) the Pt/Pd metal target used in the sputter coating process. The sample was mounted on a scanning electron microscope (SEM) equipped with an integrated EDX detector and analyzed under high vacuum conditions. A general spectrum was acquired from a selected area of the sample surface to assess the overall elemental composition. Elemental quantification was performed using the Pathfinder software and spectral data revealed characteristic peaks corresponding to platinum (Pt), palladium (Pd), and oxygen (O). In the case of the target used for Fig. 3.4a, we expect the catalytic film sputter coated in Ar to show no PtO contamination if the elemental analysis of the target doesn´t show the presence of oxygen.

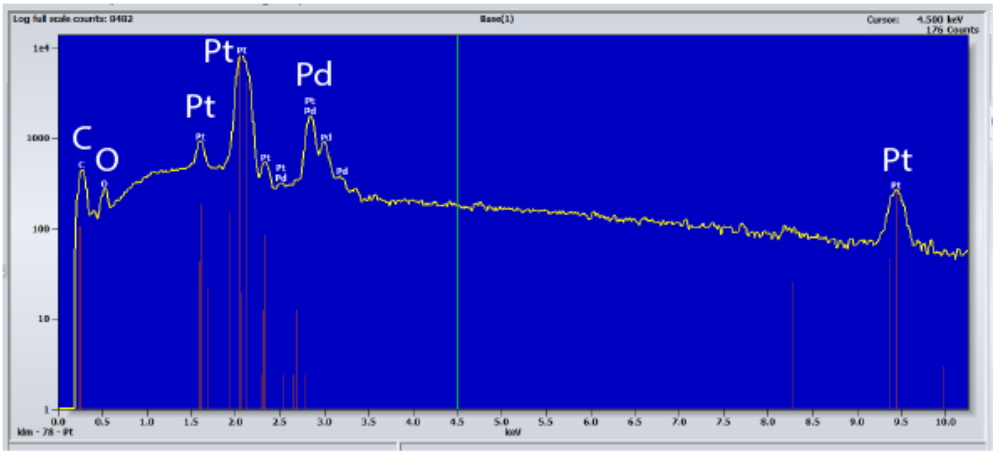

Figure 3.20: EDX spectrum of main target side that gets exposed to the plasma during sputter coating. Next to the Pt and Pd peaks, a non-negligible oxygen peak is visible which confirms contamination with PtO.

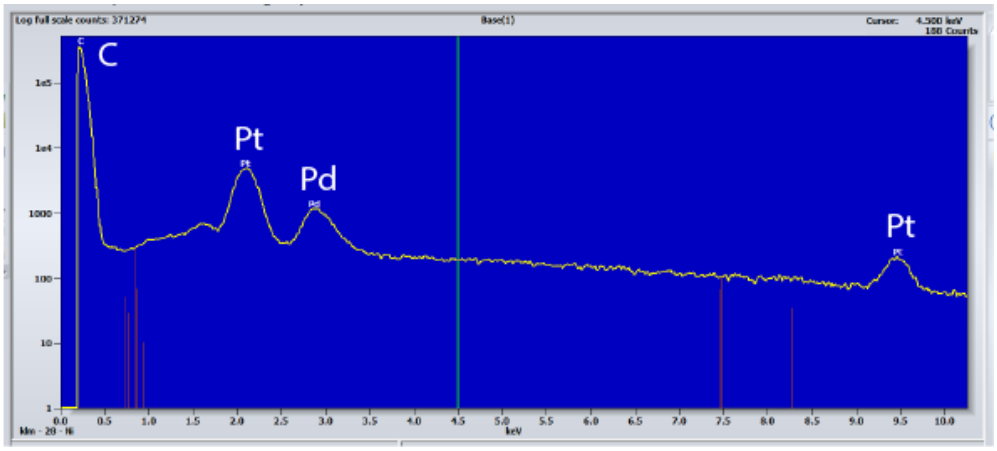

Figure 3.21: EDX spectrum of target used to prepare crescents from Fig.3a. No oxygen peak is visible and a contamination of the catalytic cap material with PtO can thus be excluded.

3.5.11 Water contact Angle of IP-Dip

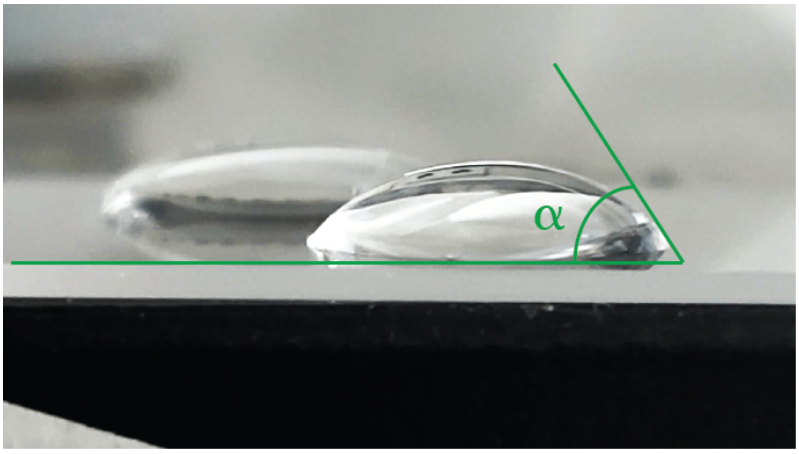

Figure 3.22: Water contact angle of IP-Dip The commercial photoresist IP-Dip (Nanoscribe GmbH) was spinn-coated on a glass substrate and cured under UV for 90 hours. The water contact angle (CA) is ca. $\sim 50^{\circ}$.

3.5.12 Zetapotential for silica-coated particles

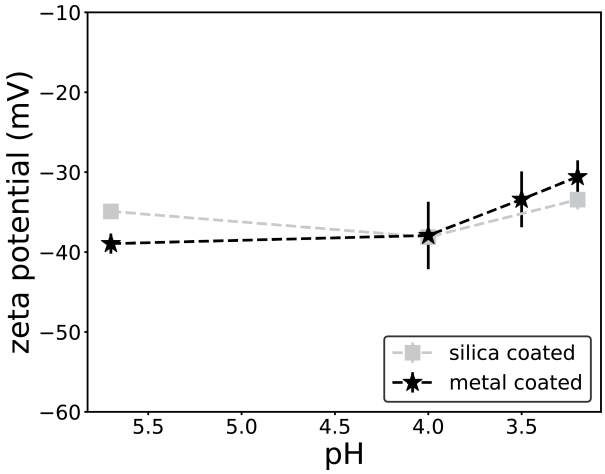

Figure 3.23: Surface zetapotential vs pH The surface zeta potential measurements for silica-coated, 3D-printed IP-Dip particles (light gray squares) were inconclusive, as the data points fall within the error bars of those measured for Pt/Pd-coated particles (black stars).

Acknowledgments

I thank Mengshi Wei for the COMSOL simulations, frequent discussions and zeta potential measurements of metal-coated and silica-coated particles. I thank Joost de Graaf, Christina Kurzthaler and Ursy Makanga for useful discussions and Rachel Doherty for support with EDX measurements.

Bibliography

[1] Howse, J. R., Jones, R. A., Ryan, A. J., Gough, T., Vafabakhsh, R., Golestanian, R. Self-Motile Colloidal Particles: From Directed Propulsion to Random Walk. *Physical Review Letters* **99** (048102).

[2] Golestanian, R., Liverpool, T. B., Ajdari, A. Propulsion of a molecular machine by asymmetric distribution of reaction products. *Physical Review Letters* **94** (22) 1–4, (2005).

[3] Ebbens, S., Gregory, D. A., Dunderdale, G., Howse, J. R., Ibrahim, Y., Liverpool, T. B., Golestanian, R. Electrokinetic effects in catalytic platinum-insulator Janus swimmers. *Epl* **106** (5).

[4] Brown, A., Poon, W. Ionic effects in self-propelled Pt-coated Janus swimmers. *Soft Matter* **10** (22) 4016–4027, (2014).

[5] Safdar, M., Wani, O. M., Jänis, J. Manganese Oxide-Based Chemically Powered Micromotors. *ACS Applied Materials and Interfaces* **7** (46) 25580–25585, (2015).

[6] Campbell, A. I., Ebbens, S. J., Illien, P., Golestanian, R. Experimental observation of flow fields around active Janus spheres. *Nature Communications* **10** (1) 1–8, (2019).

[7] Manjare, M., Wu, Y. T., Yang, B., Zhao, Y. P. Hydrophobic catalytic Janus motors: Slip boundary condition and enhanced catalytic reaction rate. *Applied Physics Letters* **104** (5).

[8] Lyu, X., Chen, J., Liu, J., Peng, Y., Duan, S., Ma, X., Wang, W. Reversing a Platinum Micromotor by Introducing Platinum Oxide. *Angewandte Chemie - International Edition* **61** (24) 1–5, (2022).

[9] Paxton, W. F., Kistler, K. C., Olmeda, C. C., Sen, A., St. Angelo, S. K., Cao, Y., Mallouk, T. E., Lammert, P. E., Crespi, V. H. Catalytic nanomotors: Autonomous movement of striped nanorods. *Journal of the American Chemical Society* **126** (41) 13424–13431, (2004).

[10] Xiao, Z., Sharan, P., Simmchen, J. Programming Tactic Behaviors of Active Colloids via Surface Charge. *ACS Nano* **19** (23) 21460–21467, (2025).

[11] van Baalen, C., Uspal, W. E., Popescu, M. N., Isa, L. Transition from scattering to orbiting upon increasing the fuel concentration for an active Janus colloid moving at an obstacle-decorated interface. *Soft Matter* **19** (45) 8790–8801, (2023).

[12] Ebbens, S. J., Howse, J. R. Direct observation of the direction of motion for spherical catalytic swimmers. *Langmuir* **27** (20) 12293–12296, (2011).

[13] Campbell, A. I., Ebbens, S. J. Gravitaxis in spherical Janus swimming devices. *Langmuir* **29** (46) 14066–14073, (2013).

[14] Sharan, P., Daddi-Moussa-Ider, A., Agudo-Canalejo, J., Golestanian, R., Simmchen, J. Pair Interaction between Two Catalytically Active Colloids. *Small* **19** (36) 1–11, (2023).

[15] Riedel, S., Hoffmann, L. A., Giomi, L., Kraft, D. J. Designing highly efficient interlocking interactions in anisotropic active particles. *Nature Communications* **15** (1) 1–9, (2024).

[16] Baker, R. D., Montenegro-Johnson, T., Sediako, A. D., Thomson, M. J., Sen, A., Lauga, E., Aranson, I. S. Shape-programmed 3D printed swimming microtori for the transport of passive and active agents. *Nature Communications* **10** (1).

[17] Liu, X., Peng, Y., Yan, Z., Cao, D., Duan, S., Wang, W. Oscillations of the Local pH Reverses Silver Micromotors in H2O2. *ChemSystemsChem* .

[18] Tan, H., Chen, B., Liu, M., Jiang, J., Ou, J., Liu, L., Wang, F., Ye, Y., Gao, J., Sun, J., Peng, F., Tu, Y. Adaptive Cu2O micromotors with pH-responsive phototaxis reversal. *Chemical Engineering Journal* **448** (May) 137689, (2022).

[19] Tong, J., Wang, D., Liu, Y., Lou, X., Jiang, J., Dong, B., Dong, R., Yang, M. Bioinspired micro/nanomotor with visible light energy-dependent forward, reverse, reciprocating, and spinning schooling motion. *Proceedings of the National Academy of Sciences of the United States of America* **118** (42) 1–7, (2021).

[20] Brooks, A. M., Tasinkevych, M., Sabrina, S., Velegol, D., Sen, A., Bishop, K. J. M. Shape-directed rotation of homogeneous micromotors via catalytic self-electrophoresis. *Nature Communications* 1–9.

[21] Michelin, S., Lauga, E. Geometric tuning of self-propulsion for Janus catalytic particles. *Scientific Reports* **7** (February) 1–9, (2017).

[22] Doherty, R. P., Varkevisser, T., Teunisse, M., Hoecht, J., Ketzetzi, S., Ouhajji, S., Kraft, D. J. Catalytically propelled 3D printed colloidal microswimmers. *Soft Matter* **16** (46) 10463–10469, (2020).

[23] Wel, C. V. D., Bhan, R. K., Verweij, R. W., Frijters, H. C., Gong, Z., Hollingsworth, A. D., Sacanna, S., Kraft, D. J. Preparation of Colloidal Organosilica Spheres through Spontaneous Emulsi fi cation .

[24] Ketzetzi, S., De Graaf, J., Kraft, D. J. Diffusion-Based Height Analysis Reveals Robust Microswimmer-Wall Separation. *Physical Review Letters* **125** (23) 1–7, (2020).

[25] Vutukuri, H. R., Preisler, Z., Besseling, T. H., Van Blaaderen, A., Dijkstra, M., Huck, W. T. Dynamic self-organization of side-propelling colloidal rods: experiments and simulations. *Soft Matter* **12** (48) 9657–9665, (2016).

[26] Kulkarni, S. A., Ogale, S. B., Vijayamohanan, K. P. Tuning the hydrophobic properties of silica particles by surface silanization using mixed self-assembled monolayers. *Journal of Colloid and Interface Science* **318** (2) 372–379, (2008).

[27] Liu, J., Xu, Y., Qiao, Z., Li, S., Ma, X., Kuang, T., Zhang, H. P., Wang, W. Quantifying and understanding the tilt of a Pt Janus active colloid near solid walls. *Soft Matter* .

[28] Ambrohewicz, D., Ciesielczyk, F., Nowacka, M., Karasiewicz, J., Piasecki, A., Maciejewski, H., Jesionowski, T. Fluoroalkylsilane versus Alkylsilane as Hydrophobic Agents for Silica and Silicates. *Journal of Nanomaterials* **2013**.

[29] Kim, J., Nason, J. A., Lawler, D. F. Influence of Surface Charge Distributions and Particle Size Distributions on Particle Attachment in Granular Media Filtration. *Environ. Sci. Technol.* **42** 2557–2562, (2008).

[30] Bechinger, C., Di Leonardo, R., Löwen, H., Reichhardt, C., Volpe, G., Volpe, G. Active particles in complex and crowded environments. *Reviews of Modern Physics* **88** (4).